

KINEMATICS OF PULSAR BEAMS

R. C. KAPOOR

Indian Institute of Astrophysics, Koramangala, Bangalore 560034, India; rck@iiap.ernet.in

AND

C. S. SHUKRE

Raman Research Institute, Sadashivanagar, Bangalore 560080, India; shukre@rri.ernet.in

Received 1997 October 2; accepted 1998 February 6

ABSTRACT

We have investigated in detail the geometry of the open magnetic field line structure of an oblique dipole rotator, with a view to attaining a better understanding of the geometry of pulsar beams in the polar cap model of pulsar emission. We find that the open field lines divide into two branches, both of which are required to describe the full polar cap. We have also investigated the possible changes in pulsar beams due to the spacetime curvature caused by the neutron star and the special relativistic aberration. Barring the light bending, which is treated numerically, we incorporate all other effects analytically. The formalism can be used for an arbitrary emission altitude and for all inclination angles between the magnetic and rotation axes. The combination of all these effects surprisingly leaves the Goldreich-Julian type beam essentially unaltered, owing to the mutually opposing nature of these effects. The general relativistic effects at most give a 4% beam squeeze. At a finer level, the possibility of seeing the resultant small effects in pulsar observations is indicated and briefly discussed.

Subject headings: pulsars: general — relativity

1. INTRODUCTION

The pulsar radio emission is currently believed to be described by the polar cap model (Radhakrishnan & Cooke 1969; Manchester & Taylor 1977). Basic ingredients in this model are charges streaming along the open magnetic field lines and the curvature radiation from these leading to pair production cascades (Goldreich & Julian 1969; Sturrock 1971). These ingredients make use of the geometry of the stellar dipole magnetic field in an essential way. In spite of numerous attempts, a satisfactory theory of the pulsar magnetosphere which could justify the use of dipole geometry still eludes us (Michel 1992). Similarly, there is no successful model of the pulsar emission given the dipole geometry (Melrose 1992). Still, the polar cap model provides the only intelligible framework for the pulsar radio emission phenomenology and therefore a plausible basis for further theoretical developments. The fairly varied geometrical possibilities provided by a magnetic dipole inclined to the pulsar rotation axis have been, surprisingly enough, not investigated in full detail. Since the arena in which the radiation mechanism must operate is the open field line region, its study may be appropriately termed the kinematics of pulsar emission. It should naturally also include other effects that are similarly kinematical in nature. These are the special relativistic aberration and the general relativistic effects due to the gravitational field of the star on the dipole geometry of the magnetic field and on propagation of light. The aberration will be important for large emission altitudes, while the gravitational effects will be felt close to the star.

The special and general relativistic effects have been previously considered only sporadically (Blaskiewicz, Cordes, & Wasserman 1991; Chen & Ruderman 1993; Kapoor 1991a; Gonthier & Harding 1994). First, we wish to explore here the extent to which they can be considered significant. Second, we have properly combined them in a comprehensive manner. In the following we develop a formalism applicable to an oblique dipole rotator that can include all these effects, and report the results of our investigations. Our intention here is not to address the dynamics of pulsar emission but to see what constraints the kinematics places on it. In § 2 we describe the detailed geometry of magnetic field lines of an oblique dipole. We show that the geometry is more intricate than considered so far (Roberts & Sturrock 1972; Biggs 1990). We find that the open field lines actually divide into two branches, a fact that seems to have escaped notice so far. In § 3 we discuss the possible modifications due to the presence of nondipolar magnetic field components. Section 4 deals with the special relativistic aberration. In §§ 5–8, the effects of the modification in the dipole magnetic field due to the stellar gravitation and the gravitational light bending on the appearance of the emission cone are considered. In § 9 we treat aberration in the presence of spacetime curvature. Finally, § 10 contains a discussion and summary of our conclusions and the implications of our results for pulsar phenomenology, e.g., the core and conal distinctions etc. (Rankin 1990, 1993).

2. THE MAGNETIC FIELD LINE GEOMETRY OF AN OBLIQUE ROTATOR

The basic assumption in the polar cap model is that the plasma surrounding the star corotates with it because of the presence of a strong dipolar magnetic field except along those field lines that pierce the velocity of the light cylinder, a cylinder whose axis is the rotation axis and has radius $r_{LC} = cP/2\pi$, where P is the pulsar period and c the velocity of light. The charges streaming along these “open” field lines are lost, and are responsible for producing the observed pulsar emission. The polar cap is thus defined to be the region on the stellar surface whose boundary is the locus of the foot of the last open field line. For a magnetic dipole aligned with the rotation axis the polar cap is circular and has the well-known half-angular size equal to

$(3/2)\theta'_{\text{GJ}}$, where (Goldreich & Julian 1969)

$$\theta'_{\text{GJ}} = \sin^{-1} \left(\frac{R_*}{r_{\text{LC}}} \right)^{1/2} \quad (1)$$

and R_* is the neutron star radius. We assume the magnetic field line structure of a radio pulsar to be purely dipolar in nature and discuss the effect of possible nondipolar components in the next section. Let the oblique rotator be at an inclination angle α to the rotation axis. We define the rotational coordinate system as the one in which the rotation axis is the z -axis, and the magnetic coordinate system as the one with the magnetic axis as the z' -axis. The magnetic and rotation axes are taken to lie in the (y', z') -plane, which is the same as the (y, z) -plane. In terms of magnetic coordinates (r, θ', φ') , the relevant magnetic field components are

$$B_r = \frac{2\mu_0}{r^3} \cos \theta', \quad B_{\theta'} = \frac{\mu_0}{r^3} \sin \theta', \quad B_{\varphi'} = 0. \quad (2)$$

Here μ_0 is the stellar dipole moment. In the rotational coordinates, the field components are

$$B_r = \frac{2\mu_0}{r^3} (\cos \alpha \cos \theta + \sin \alpha \sin \theta \sin \varphi), \quad (3)$$

$$B_{\theta} = \frac{\mu_0}{r^3} (\cos \alpha \sin \theta - \sin \alpha \cos \theta \sin \varphi), \quad (4)$$

$$B_{\varphi} = -\frac{\mu_0}{r^3} \sin \alpha \cos \varphi. \quad (5)$$

Figure 1 shows the dipole field line geometry, drawn here in the plane $\varphi = \pi/2$. Field lines tangent to the light cylinder (radius r_{LC}) at points B and B' are the last open field lines for a particular inclination. For any given longitude φ_c , the field

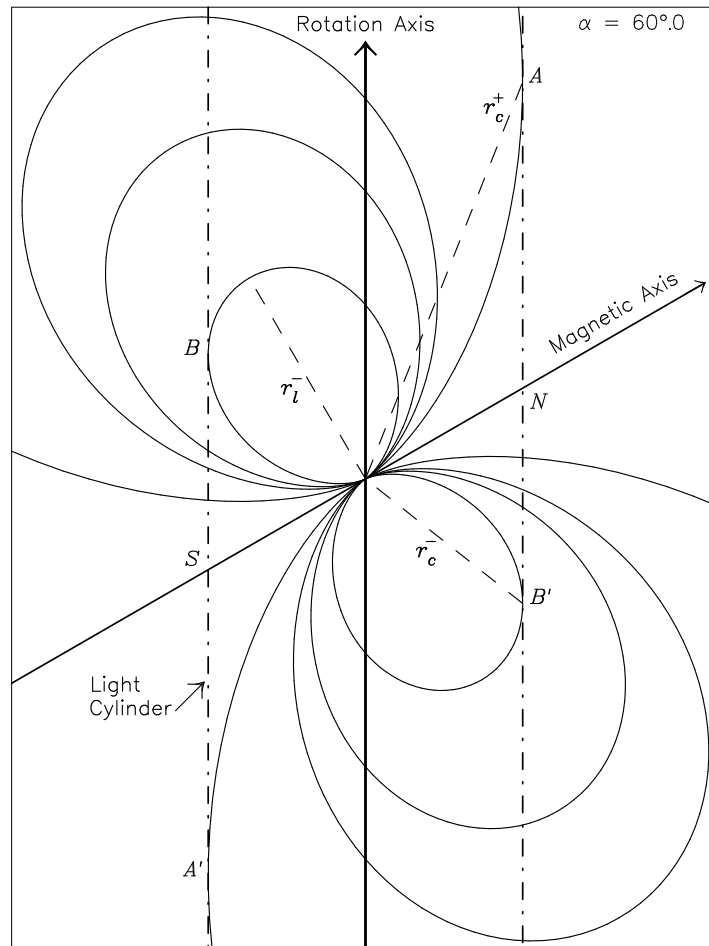


FIG. 1.—Plot of magnetic field lines of an oblique dipole, in the plane containing the rotation and magnetic axes. The lines contained between N and A pertain to the θ_c^+ root, while those between B and B' pertain to the θ_c^- root (see text).

component normal to the light cylinder is zero for tangent field lines, i.e.,

$$B_\rho = B_r \sin \theta + B_\theta \cos \theta = 0. \quad (6)$$

Consequently the following relation results, giving the polar angle θ_c of the tangent point on the field line in terms of α and φ_c :

$$2W_c \tan^2 \theta_c + 3 \tan \theta_c - W_c = 0, \quad (7)$$

where $W_c = \tan \alpha \sin \varphi_c$. This quadratic equation has two roots, describing two branches of the last open field lines:

$$\tan \theta_c^\pm = -\frac{3}{4W_c} \left[1 \mp \left(1 + \frac{8W_c^2}{9} \right)^{1/2} \right]. \quad (8)$$

In Figure 1 (i.e., for $\varphi_c = \pi/2$) the θ_c^+ root pertains to open field lines contained between the points N and A . The θ_c^- root pertains to open field lines between the points B and B' . Since we are concerned with only one of the magnetic poles, the roots have ranges so adjusted that

$$0 \leq \theta_c^+ \leq \theta_0, \quad (9)$$

$$\pi/2 \leq \theta_c^- \leq \pi - \theta_0, \quad (10)$$

where $\theta_0 = \tan^{-1} (2^{-1/2})$. It should be noted that for θ_c^+ we have $0 \leq \varphi_c \leq \pi$, while for θ_c^- , φ_c covers the entire 2π range. It is clear from the geometry in Figure 1 that the tangent point is located at

$$r_c^\pm = \frac{r_{\text{LC}}}{\sin \theta_c^\pm}, \quad (11)$$

so that the equatorial radius r_l of the last open field line is

$$r_l^\pm = \frac{r_c}{\sin^2 \theta_c} \Big|_{\pm} = \frac{r_{\text{LC}}}{\sin \theta_c \sin^2 \theta_c} \Big|_{\pm}. \quad (12)$$

From $(r_c^\pm, \theta_c^\pm, \varphi_c)$, we can derive the magnetic coordinate values $(r_c^\pm, \theta_c^\pm, \varphi_c^\pm)$. These are then traced backward along the magnetic field lines using the equation

$$\frac{\sin^2 \theta'}{r} = \frac{1}{r_l}. \quad (13)$$

An extrapolation using this relation leads us to points $(r_e, \theta'_e, \varphi'_e)$ that define the boundary of the emission zone. Thus θ'_e is the opening angle of the emission zone. Since the radiation is supposed to emanate tangential to open magnetic field lines, the radiation cone is wider. We refer to this as the *emission cone*. When $r_e = R_*$, this is usually referred to as the polar cap. It is defined by directions (θ'_r, φ'_r) , where

$$\theta'_r = \theta'_e + \mu'_e, \quad (14)$$

$$\varphi'_r = \varphi'_e = \varphi'_c. \quad (15)$$

The quantity μ'_e in equation (14) is the angle between the radial direction and the tangent to the field line. We shall refer to μ'_e as the tangent angle. It is given by the usual relation

$$\tan \mu'_e = \frac{1}{2} \tan \theta'_e. \quad (16)$$

For radiation originating near the star $\theta'_r = \frac{3}{2}\theta'_e$ provides an excellent approximation.

From Figure 1, what is not obvious is how the field lines defining the boundary of the θ_c^+ region will look for other values of φ_c . However, in Figure 2, for $\alpha = 75^\circ$ and a typical pulsar period $P = 2^{-1/2}$ s, we depict the locus of the feet of the field lines that define the boundaries of θ_c^+ and θ_c^- regions of the polar cap for both the poles. For the north pole both θ_c^+ and θ_c^- branches are shown as polar plots in Figure 3 for various inclination angles α and the same pulsar period and r_e . The radial and azimuthal coordinates in Figures 2 and 3 are θ'_r and φ'_r , respectively. For a different value of P similar diagrams can be obtained simply by rescaling the axes. Similarly, if the emission is assumed to originate not at the surface but at the radial height r_e , then again the diagram can be rescaled by a factor $(r_e/R_*)^{1/2}$ provided that $r_e/R_* \lesssim 1000$. The discussion of pulsar polar caps hitherto had not distinguished between the two branches of open field lines (e.g., Biggs 1990). It should be noted that in the θ_c^+ region, the field lines that are tangent to the light cylinder nevertheless pierce it at some other location, unlike the θ_c^- case. The region of the polar cap defined by the θ_c^+ solution grows in size with increasing α but still stays within the boundary defined by the θ_c^- solution provided that $\alpha \neq \pi/2$ (see later). Thus, although the total extent of the polar cap is unaffected by the presence of the θ_c^+ region, it selects out a part of it. As will be seen, this part has several notable features. It has a peculiar triangular shape whose lowest vertex is on the magnetic axis for all values of α . We wish to emphasize that a complete description of the polar cap necessarily requires both the solutions. Although for $\alpha < \pi/2$, the θ_c^+ region is always contained within the θ_c^- region, at $\alpha = \pi/2$ a striking feature is noticed. While the θ_c^- region assumes a shape like the symbol for "infinity" (i.e., ∞), the θ_c^+ region becomes two-sided and smoothly fills up the notches (see Fig. 4). Thus, in the orthogonal

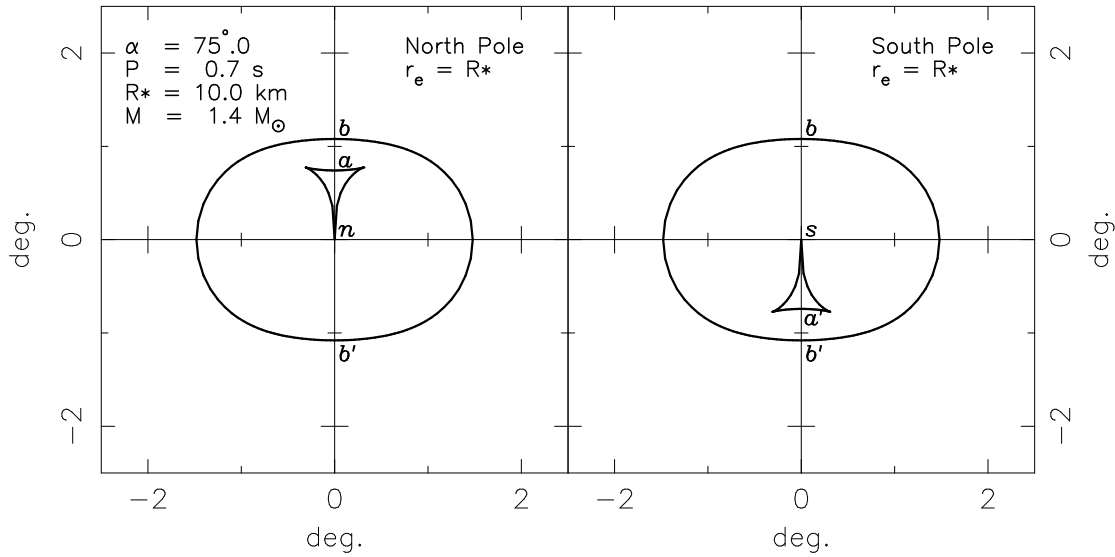


FIG. 2.—Polar plots for $\alpha = 75^\circ$, $P = 2^{-1/2}$ s, and $r_e = R_*$ showing the polar caps for the north and the south poles. The points identified by lowercase a , b , b' , n and s are counterparts of points labeled similarly by uppercase letters in Fig. 1.

case, the polar cap boundary cannot be correctly delineated unless both solutions are considered and not just the θ_c^- solution. The emission cone shapes in the orthogonal case which have been considered so far include both the θ_c^+ and the θ_c^- regions without identifying them as distinct.

One of the characteristics of the polar diagram in Figure 3 is that the emission cone shows a latitudinal compression as α increases. This has been known for some time (Roberts & Sturrock 1972; Biggs 1990). This compression is described by the

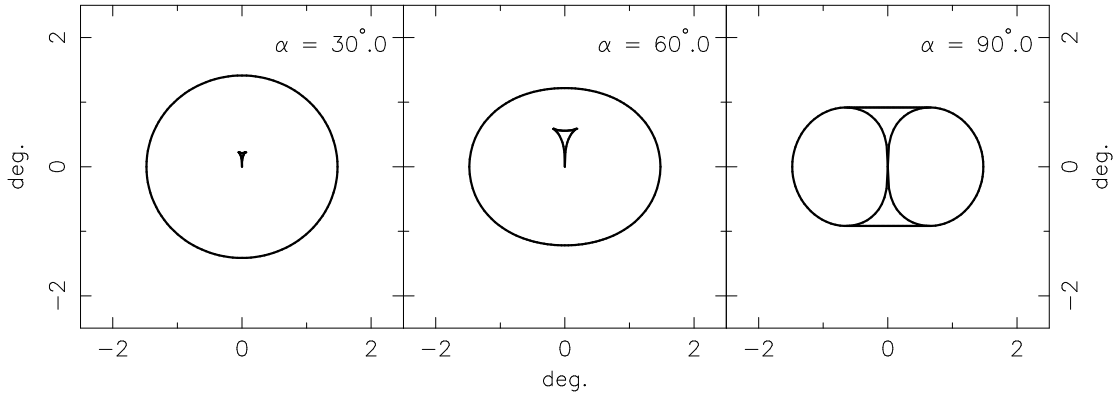


FIG. 3.—Polar caps for $P = 2^{-1/2}$ s, $R_* = 10.0$ km, $r_e = R_*$, and $\alpha = 30^\circ, 60^\circ$, and 90°

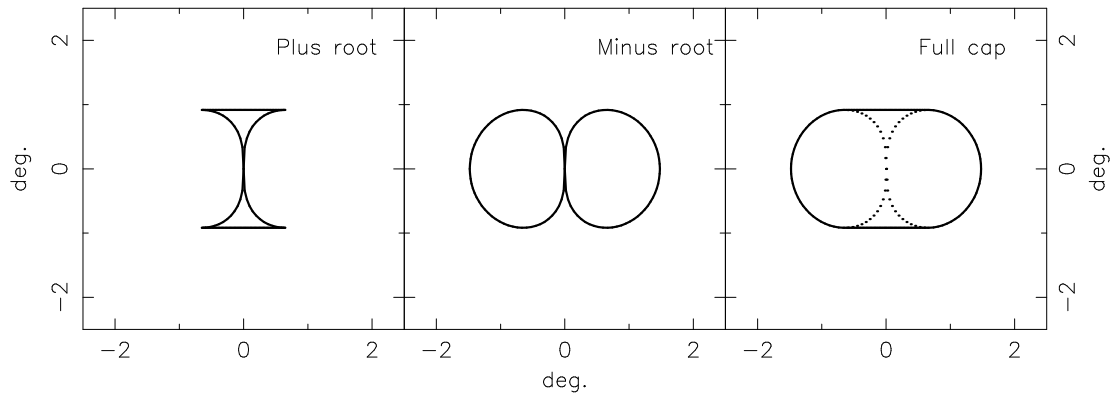


FIG. 4.—Polar cap regions for $\alpha = 90^\circ$, $P = 2^{-1/2}$ s, $R_* = 10.0$ km, $r_e = R_*$, showing the θ_c^+ region, the θ_c^- region, and the full polar cap

ratio R_c of the maximum latitudinal extent of the emission cone to its maximum longitudinal one. It is given by

$$R_c = [\theta'_m + \tan^{-1}(\frac{1}{2} \tan \theta'_m)] / [\theta'_0 + \tan^{-1}(\frac{1}{2} \tan \theta'_0)], \quad (17)$$

where θ'_0 is the analog, for $r_e > R_*$, of θ'_{GJ} , i.e., $\sin^2 \theta'_0 = r_e/r_{LC}$; and

$$\sin^2 \theta'_m = (r_e/r_{LC}) \cos \alpha_+ \cos^2 \alpha_-. \quad (18)$$

The angles α_{\pm} are defined as

$$\alpha_{\pm} = \frac{1}{2}[\alpha \pm \sin^{-1}(\frac{1}{3} \sin \alpha)]. \quad (19)$$

It should be noted that for $\alpha \neq \pi/2$, R_c pertains to the θ_c^- region. For $\alpha = \pi/2$, it is contributed solely by the θ_c^+ region because the corresponding value for the θ_c^- region is zero. The formula for R_c in equation (17) reduces to the one given by Kijak & Gil (1997) in the limit of small α . The latitudinal compression is maximum at $\alpha = \pi/2$. At the stellar surface it amounts to $R_c = 0.62$ for $\alpha = \pi/2$ and to $R_c = 0.82$ for $\alpha = \pi/3$. For $\alpha = 0$ there is no compression at all ($R_c = 1$). In contrast to the compression of the emission cone, the θ_c^+ region shows another notable feature, a latitudinal elongation as α increases. This elongation can be described by the ratio R_c^+ of the maximum latitudinal extent of the θ_c^+ region to the maximum longitudinal extent of the emission cone. It is given by

$$R_c^+ = [\theta_m'^+ + \tan^{-1}(\frac{1}{2} \tan \theta_m'^+)] / [\theta_0' + \tan^{-1}(\frac{1}{2} \tan \theta_0')], \quad (20)$$

where

$$\sin^2 \theta_m'^+ = (r_e/r_{LC}) \sin \alpha_- \sin^2 \alpha_+. \quad (21)$$

In the aligned case the θ_c^+ region reduces to a point. For intermediate inclinations it does not play a role in determining the emission cone boundary. However, in the orthogonal case it becomes indispensable as noted above. Thus yet another notable feature of the θ_c^+ region is its sensitive dependence on α . In the following the θ_c^+ region is always featured in the figures along with the θ_c^- region. This is to emphasize the fact that even though usually it occurs inside the θ_c^- region, it is a distinguishable part within the emission cone. As described later, the emission cone changes due to the inclusion of various physical effects. These changes are not confined to the boundary of the emission cone, and the depiction of the θ_c^+ region demonstrates how they occur in the inner region. Last, it should be noted that for $r_e = \frac{2}{3}r_{LC}$, the θ_c^- region covers a solid angle of 2π , which is certainly not meaningful in the context of the polar cap model. Therefore, unless some additional effects are invoked, emission altitudes associated with the θ_c^- region should be less than $\frac{2}{3}r_{LC}$. This restriction does not apply to the θ_c^+ region. The θ_c^+ region is qualitatively similar to the emission region as indicated by the ‘‘favorably’’ curved magnetic field lines (Scharlemann, Arons, & Fawley 1978; Arons 1979). Although of great interest, further exploration of this connection is beyond the scope of the present work, which is restricted to the kinematics. We have considered it partially in Kapoor & Shukre (1998, hereafter KS III).

3. THE EFFECT OF NONDIPOLAR MAGNETIC FIELDS

At this juncture it is appropriate to examine how the nondipolar magnetic field components may affect the beam shapes that we have described so far. One possible nondipolar field geometry which can be invoked is that of an off-center dipole (Arons 1996). This we do not consider, for reasons of simplicity. Our results for the pure dipolar case will, however, be indicative of those in the off-center one. Apart from this there are two possible components that can be considered. First, the stellar magnetic field may have higher multipoles. Second, the magnetospheric currents are expected to give rise to toroidal magnetic fields. Before we turn to their discussion, we recapitulate here the procedure of the last section for deriving the emission cone. We first define a region using equation (8), which essentially is the image on the light cylinder of the emission zone at an altitude r_e . The second step involves a tracing back of this region using the magnetic field geometry as in equation (13). This leads us to the emission zone defined by values of (θ'_e, φ'_e) . Last, we modify for tangential emission along the magnetic field line using equation (14) to obtain (θ'_e, φ'_e) .

We first consider nondipolar stellar magnetic field components. The issue of such components has been discussed in detail by Arons (1993), where it is concluded that ‘‘there is no clear evidence either theoretical or observational for large scale nondipolar field in any pulsar.’’ Even so, since at large distances multipolar components die out faster than the dipole ones, small multipole admixtures will modify not equation (8) but only equations (13) and (14), and that too near the stellar surface. Any quantitative assessment will require the details of the magnetic field. But still, if the pulsar emission originates at altitudes of a few R_* or more (see Rankin 1993), then we would expect our description to be adequate. Let us now consider the toroidal field components. The only estimate available for these comes from pulsar spin-down rates and indicates that the dipole and toroidal fields (say, B_d and B_t , respectively) are comparable at the light cylinder (Sturrock 1971; see also Shitov 1985). We can therefore write in an approximate fashion

$$B_t = B_0 \left(\frac{R_*}{r_{LC}} \right)^3 \left(\frac{r}{r_{LC}} \right)^n \quad (22)$$

and

$$B_d = B_0 \left(\frac{R_*}{r} \right)^3, \quad (23)$$

where B_0 is the surface magnetic field strength and all we require is that $n > 0$. Now as far as equation (8) is concerned, the presence of B_t leaves it unchanged because tangentiality involves only the component B_ρ . Therefore the emission-zone image

on the light cylinder is unaffected. Equations (13) and (14) may no longer seem appropriate to trace back and derive the emission cone. But as we have noted above, observations constrain the emission altitudes for the θ_c^- region to $\ll \frac{2}{3}r_{LC}$. Consequently, from equations (22) and (23) above, we see that for $r = \frac{2}{3}r_{LC}$ the maximum value of B_t is $0.2B_d$ (for $n = 1$). Thus we expect $B_t \ll 0.2B_d$ for $r \ll \frac{2}{3}r_{LC}$, and we still would not expect much change compared to the pure dipolar case. The θ_c^+ region is normally very small, and if a higher emission altitude is associated with it, the effect of B_t on it will be uniform and only shift it in azimuth φ as a whole in a sense opposite to that of stellar rotation. Note that aberration, which we consider later, will introduce an opposite shift.

4. THE EFFECT OF ABERRATION ON THE PULSAR BEAM

Although the initial proposal of the polar cap model had $r_e = R_*$, higher altitudes have been suggested (e.g., Phillips 1992; Rankin 1993). In such a case aberration should be included. To incorporate effects of aberration on the pulsar beam, let us consider an arbitrary point within the emission cone. Its corotational velocity in the rotational coordinates (r, θ, φ) is

$$v = \frac{r_e \Omega \sin \theta_e}{c} = \frac{r_e}{r_{LC}} \sin \theta_e. \quad (24)$$

To be precise, the velocity here needs to be scaled by the gravitational redshift factor, $(1 - 2m/r_e)^{-1/2}$. In subsequent sections dealing with spacetime curvature effects, this scaling is incorporated in an automatic manner, though it is not significant. The rotational frame Cartesian coordinates (x, y, z) are related to in the magnetic ones through

$$x_e = x'_e, \quad y_e = y'_e \cos \alpha + z'_e \sin \alpha, \quad (25)$$

$$z_e = z'_e \cos \alpha - y'_e \sin \alpha. \quad (26)$$

For the unit vector (θ_e, φ_e) , we have

$$\sin^2 \theta_e = x_e'^2 + y_e'^2 \quad (27)$$

and

$$\tan \varphi_e = \frac{y_e}{x_e} = \frac{\sin \theta'_e \sin \varphi'_c \cos \alpha + \cos \theta'_e \sin \alpha}{\sin \theta'_e \cos \varphi'_c}. \quad (28)$$

One can construct similar quantities, such as

$$\sin \theta_r = (x_r'^2 + y_r'^2)^{1/2} \quad (29)$$

and

$$\tan \varphi_r = y_r/x_r'. \quad (30)$$

The direction cosines in the rotational frame at the emission point are

$$l_r = \cos \theta_r \cos \theta_e + \sin \theta_r \sin \theta_e \cos (\varphi_r - \varphi_e), \quad (31)$$

$$m_r = -\cos \theta_r \sin \theta_e + \sin \theta_r \cos \theta_e \cos (\varphi_r - \varphi_e), \quad (32)$$

$$n_r = \sin \theta_r \sin (\varphi_r - \varphi_e). \quad (33)$$

We denote the changed form of any quantity (e.g., l_r) after aberration by adding a caret on top of it (e.g., \hat{l}_r). Thus the direction cosines as measured in the reference frame of the inertial observer are \hat{l}_r, \hat{m}_r , and \hat{n}_r such that

$$\hat{l}_r = \cos \hat{\theta}_r \cos \theta_e + \sin \hat{\theta}_r \sin \theta_e \cos (\hat{\varphi}_r - \varphi_e) = \frac{l_r}{\gamma(1 + vn_r)}, \quad (34)$$

$$\hat{m}_r = -\cos \hat{\theta}_r \sin \theta_e + \sin \hat{\theta}_r \cos \theta_e \cos (\hat{\varphi}_r - \varphi_e) = \frac{m_r}{\gamma(1 + vn_r)}, \quad (35)$$

$$\hat{n}_r = \sin \hat{\theta}_r \sin (\hat{\varphi}_r - \varphi_e) = \frac{n_r + v}{(1 + vn_r)}, \quad (36)$$

where γ is the usual Lorentz factor for the corotating emission point, $\gamma = (1 - v^2)^{-1/2}$. Thus the aberrated values $(\hat{\theta}_r, \hat{\varphi}_r)$ of the angles (θ_r, φ_r) are given by

$$\cos \hat{\theta}_r = \frac{\cos \theta_r}{\gamma[1 + v \sin \theta_r \sin (\varphi_r - \varphi_e)]} = (1 + z) \cos \theta_r, \quad (37)$$

and

$$\tan (\hat{\varphi}_r - \varphi_e) = \frac{\gamma[\sin \theta_r \sin (\varphi_r - \varphi_e) + v]}{\sin \theta_r \cos (\varphi_r - \varphi_e)}, \quad (38)$$

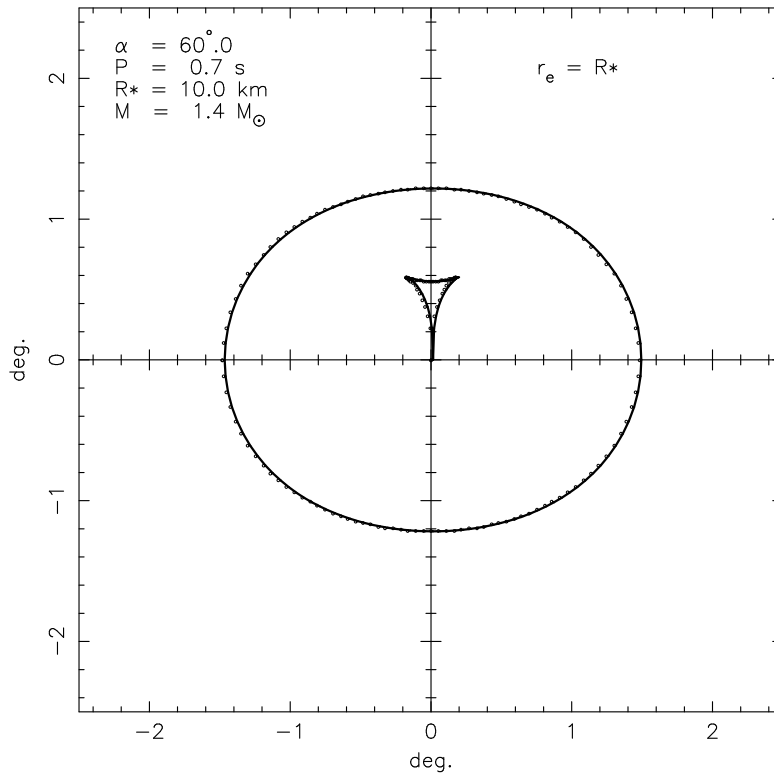


FIG. 5.—Polar cap for $\alpha = 60^\circ$, $P = 2^{-1/2}$ s, with (solid line) and without (dots) aberration

where the Doppler redshift factor is

$$1 + z = \frac{v_e}{\hat{v}} = \gamma(1 + v\hat{n}_r) . \tag{39}$$

One can transform the $\hat{\theta}_r$ and $\hat{\phi}_r$ values to the magnetic coordinates through

$$\sin \hat{\theta}'_r \cos \hat{\phi}'_r = \sin \hat{\theta}_r \cos \hat{\phi}_r , \tag{40}$$

$$\sin \hat{\theta}'_r \sin \hat{\phi}'_r = \sin \hat{\theta}_r \sin \hat{\phi}_r \cos \alpha - \cos \hat{\theta}_r \sin \alpha , \tag{41}$$

$$\cos \hat{\theta}'_r = \cos \hat{\theta}_r \cos \alpha + \sin \hat{\theta}_r \sin \hat{\phi}_r \sin \alpha . \tag{42}$$

A polar plot of the aberrated pulsar beam as seen by an inertial observer can be obtained from $\hat{\theta}'_r$ and $\hat{\phi}'_r$ for any inclination angle α . In Figure 5 we show the emission cone for $r_e = R_*$ with and without aberration. It is clear that at the stellar surface the effect of aberration is just to shift the whole emission cone by a small angle v in azimuth ϕ . We show in Figure 6 the polar plots for various emission heights. The emission cone, in addition to the shift, undergoes a twist around the magnetic axis which is noticeable at higher emission altitudes. This is due to the variation in corotation velocity over the emission cone. It should, however, be kept in mind that when not scaled by $(R_*/r_e)^{1/2}$, the emission cone in Figure 6 for $r_e \cong 2250R_* = \frac{2}{3}r_{LC}$ has

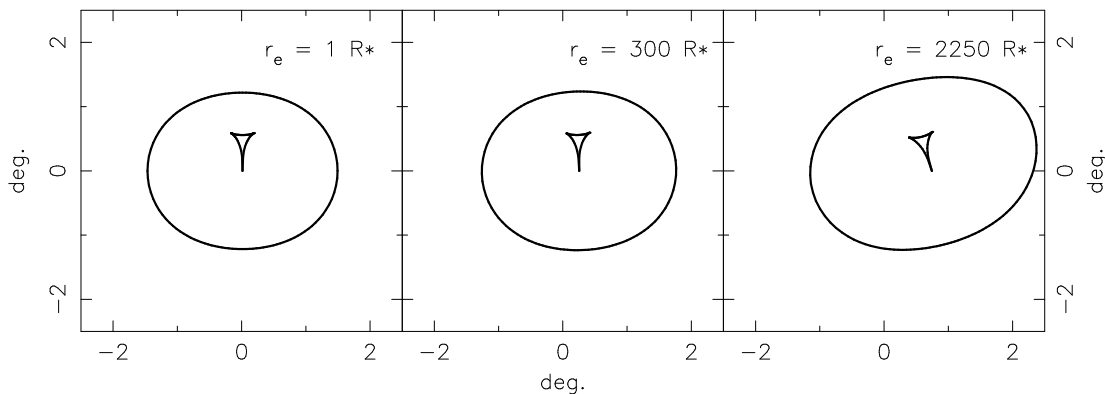


FIG. 6.—Emission cones for $\alpha = 60^\circ$, $P = 2^{-1/2}$ s, $R_* = 10.0$ km, after aberration at altitudes r_e of 1, 300, and $2250R_*$. Angular extents are multiplied by the factor $(R_*/r_e)^{1/2}$.

an extent of 180° . Note that our figure in such cases is not truly representative of the emission cone. In our literal interpretation of the polar cap model, the emission cone at altitudes larger than $\frac{2}{3}r_{LC}$ has a vast angular size over which the corotation velocity also varies over a large range. Consequently the aberrated pulsar beam does not display substantial shrinking. Therefore, emission altitudes larger than $\frac{2}{3}r_{LC}$ are still not meaningful. On the other hand, if a small portion of the full cone, e.g., the θ_c^+ region, is considered, emission altitudes larger than $\frac{2}{3}r_{LC}$ can still be relevant, and significant aberration effects would be seen.

5. THE GRAVITATIONAL EFFECTS

The emission region is usually thought to be located near the neutron star precisely where the gravitational effects of a curved spacetime would be maximum. In our kinematical considerations two effects are relevant. First, because of the curvature of spacetime, the geometry of the magnetic field is modified, the effect amounting to what can be called a “squeezing” of the field. Second, light rays are not straight but bent, an effect henceforth referred to as “bending.” It can perhaps be argued that for a rotating neutron star it would be most appropriate to use the Kerr metric (Chandrasekhar 1983) to calculate these general relativistic effects. However, the amount of rotation is generally small, and the deviations from the nonrotating Schwarzschild case are expected to be small. For the effect of gravitation on the stellar magnetic field the solutions are known in the Schwarzschild (see later) or the aligned Kerr case (Chitre & Vishveshvara 1975; Petterson 1975). We consider only the Schwarzschild case. To include the bending of light, we consider the Schwarzschild case first and comment later on corrections that would arise if the Kerr metric were used. The discussion of gravitational effects is usually presented in terms of the so-called Schwarzschild coordinates $(t_g, r_g, \theta_g, \varphi_g)$. In terms of these, the Schwarzschild line element is

$$ds^2 = (1 - 2m/r_g)dt_g^2 - (1 - 2m/r_g)^{-1}dr_g^2 - r_g^2(d\theta_g^2 + \sin^2\theta_g d\varphi_g^2), \quad (43)$$

where $m = GM/c^2$ and M is the mass of the star. We identify t_g and r_g with our t and r . The angles (θ_g, φ_g) are identified with our magnetic coordinates (θ', φ') in different ways for “squeezing” and “bending” according to convenience as described below.

6. MAGNETIC FIELD GEOMETRY IN THE SCHWARZSCHILD BACKGROUND

To consider the effect of spacetime curvature on the dipole magnetic field, we use the general relativistic solution for a magnetic dipole field in an external Schwarzschild background (Ginzburg 1964; Petterson 1974; Wasserman & Shapiro 1983), which gives the components of the magnetic field as measured by the observer relevant here and locally at rest. For discussing the changed field line geometry we identify φ_g and θ_g with φ' and θ' respectively. Because of the axisymmetry all quantities are independent of φ' . Thus the nonzero (tetrad) field components are

$$B_{\theta'} = \frac{6\mu_0 \sin \theta'}{r^3} \left[\left(\frac{r}{2m} \right)^3 \left(1 - \frac{2m}{r} \right)^{1/2} \ln \left(1 - \frac{2m}{r} \right) + \left(\frac{r}{2m} \right)^2 \frac{1 - m/r}{(1 - 2m/r)^{1/2}} \right] = \frac{6\mu_0 \sin \theta'}{r^3} b_{\theta}(r), \quad (44)$$

and

$$B_r = -\frac{6\mu_0 \cos \theta'}{r^3} \left[\left(\frac{r}{2m} \right)^3 \ln \left(1 - \frac{2m}{r} \right) + \left(\frac{r}{2m} \right)^2 \left(1 + \frac{m}{r} \right) \right] = -\frac{6\mu_0 \cos \theta'}{r^3} b_r(r), \quad (45)$$

where μ_0 is identified as the stellar magnetic dipole moment. If one defines a line of force as the tangent to the direction of the magnetic field, then its equation is

$$\left(1 - \frac{2m}{r} \right)^{1/2} r \frac{d\theta'}{dr} = \frac{B_{\theta'}}{B_r}, \quad (46)$$

where

$$\frac{B_{\theta'}}{B_r} = -\frac{b_{\theta'}}{b_r} \tan \theta' = f(r) \tan \theta'. \quad (47)$$

The function $f(r)$ measures the departure from a dipole magnetic field in a flat spacetime such that the field lines now crowd closer near the poles. Hence we use the nomenclature “squeezing.” Now the field lines are described by

$$r \frac{d\theta'}{dr} = \frac{f(r) \tan \theta'}{(1 - 2m/r)^{1/2}}. \quad (48)$$

Equations (48) can be integrated, and we find the equation for the field line to be

$$\frac{\sin^2 \theta'}{r} = \frac{b_r(r_L)}{b_r(r)} \frac{1}{r_L}, \quad (49)$$

where r_L is the equatorial radius of the field line (i.e., the value of r for which $\theta' = \pi/2$). Note that uppercase subscripts are used to denote the curved spacetime quantities to distinguish them from their flat spacetime counterparts, which carry lowercase subscripts. The equations in the flat spacetime are recovered by putting $f(r) = 0.5$ or $b_r(r) = -\frac{1}{3}$. However, it should be kept in mind that the field line with a given value of r_L does not go over in the flat spacetime case to a field line with the same value of r_l . In this case, therefore, we have to solve also for r_L . Except for the aligned case (considered by Kapoor 1991b; Gonthier &

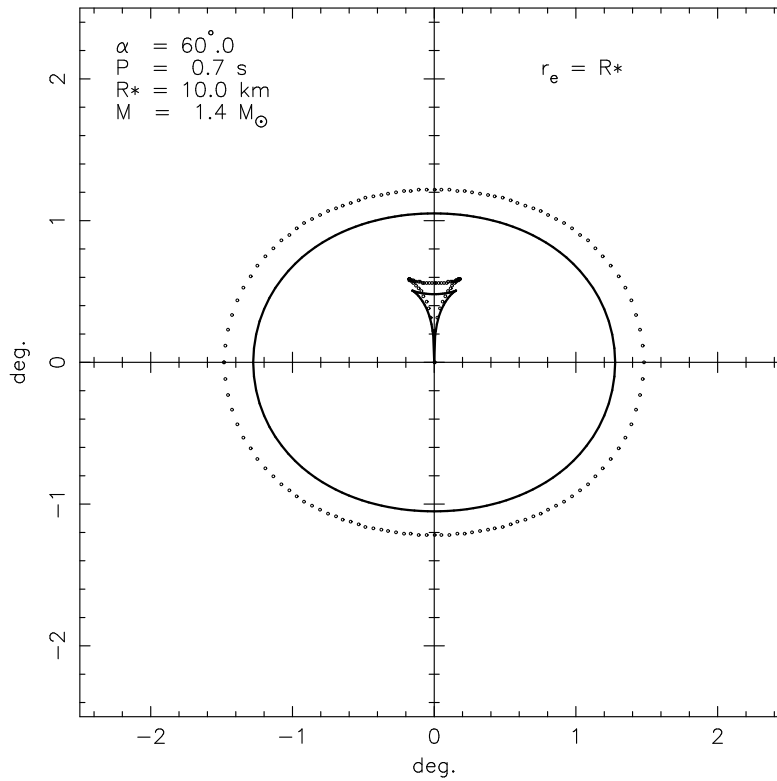


FIG. 7.—The outer curve (dots) is the flat spacetime polar cap. The inner curve (solid line) shows the polar cap squeezed by the general relativistic magnetic field “squeezing.” The stellar mass and radius are $1.4 M_\odot$ and 10 km, respectively.

Harding 1994), this is an involved procedure. As before, field lines that are of interest are the ones which are tangent to the light cylinder. In this case we can redo the calculation of § 2 to find the tangent points. We get the following equation (which replaces eq. [7]):

$$W_c \tan^2 \theta_c + (1 + f_c) \tan \theta_c - f_c W_c = 0, \quad (50)$$

where $f_c = f(r_c)$. The solutions are

$$\tan \theta_c^\pm = \frac{-(1 + f_c) \pm [(1 + f_c)^2 + 4f_c W_c^2]^{1/2}}{2W_c}, \quad (51)$$

and, as before,

$$r_c^\pm = \frac{r_{LC}}{\sin \theta_c^\pm}. \quad (52)$$

It is clear that, in contrast to the flat spacetime case, θ_c^\pm and r_c^\pm are to be simultaneously solved for, using equations (51) and (52). A simplification occurs, however, because $r_c^\pm \geq r_{LC}$. The smallest value of r_{LC} we encounter is 74 km for the millisecond pulsar. For $M = 1.4 M_\odot$ and values of r larger than 74 km, $f(r)$ differs from its flat spacetime value of 0.5 at most by 0.008. It can be shown that θ_c , the value derived after squeezing, can differ from θ_c , the flat spacetime value, at most by $0^\circ.22$, and

$$\frac{r_c - r_c}{r_c} \leq 0.004. \quad (53)$$

This is furthermore true for all values of α . Therefore, as far as determination of θ_c and r_c is concerned, we can simply take over the flat spacetime values of θ_c and r_c from § 2. It is now required to extrapolate these values along field lines given by equation (49) and derive θ'_E . For this purpose, we can write equation (49) in the following more convenient form so that we do not need to solve for r_L :

$$\frac{\sin^2 \theta'_E}{r_e} = \frac{b_r(r_{LC})}{b_r(r_e)} \frac{\sin^2 \theta'_C}{r_{LC}}. \quad (54)$$

We can get a rough idea of how much θ'_E will change due to squeezing as follows. From equation (53) and because $r_l \gtrsim r_c$, we see that $r_L \cong r_b$, and we can write $b_r(r_L) = -\frac{1}{3}$. Therefore,

$$\sin^2 \theta'_E = \frac{-1}{3b_r(r_e)} \sin^2 \theta'_e. \quad (55)$$

For $r_e = R_*$, this leads to

$$\sin \theta'_E = 0.81 \sin \theta'_e, \quad (56)$$

or $\theta'_E = 0.81\theta'_e$. Values of θ'_E after the full computation using equation (54) are found to be very close to this estimate. The angle μ'_E made by the tangent to a magnetic line of force with the radius vector at the emission point now is given by

$$\tan \mu'_E = \frac{B_{\theta'}}{B_r} \Big|_{r_e} = f(r_e) \tan \theta'_E. \quad (57)$$

The opening angle of the pulsar beam is now smaller than that given by equation (14):

$$\theta'_R = \theta'_E + \mu'_E = \theta'_E + \tan^{-1} [f(r_e) \tan \theta'_E]. \quad (58)$$

Also, as before,

$$\varphi'_R = \varphi'_c. \quad (59)$$

In the asymptotic limit (i.e., $r \rightarrow \infty$), one is led to the familiar relations for flat spacetime,

$$\sin \theta'_E \rightarrow \sin \theta'_e = \left(\frac{r_e}{R_*} \right)^{1/2} \sin \theta'_{GJ} = \left(\frac{r_e}{r_{LC}} \right)^{1/2} \quad (60)$$

and

$$\theta'_R \rightarrow \theta'_r = \theta'_e + \tan^{-1} \left(\frac{1}{2} \tan \theta'_e \right) \simeq \frac{3}{2} \theta'_e. \quad (61)$$

It should be noted that this effect depends only on the ratio m/r_e and not on P , α , or B_0 . For $M = 1.4 M_\odot$ ($m = 2.1$ km), and $R_* = 10$ km, and $r_e = R_*$, θ'_e , the emission zone opening angle is reduced by 19% of its flat spacetime value, the tangent angle μ'_e is reduced by 4%, leading to a net reduction in the emission cone angle θ'_r of about 14% due to the field squeeze. This is shown in Figure 7 for a typical case. For $r_e = 2R_*$ and $5R_*$, the emission cone shrinks by 6.5% and 2.5%, respectively. Thus for values of $r_e \gtrsim 5R_*$ “squeezing” has negligible effect.

7. LIGHT PROPAGATION IN CURVED SPACETIME

Gravitational bending of light has been considered previously in the context of pulsar emission by many authors (Kapoor 1991a and references therein; Chen & Ruderman 1993; Gonthier & Harding 1994; Kapoor & Shukre 1995). Our treatment of this effect displays how the shape and size of the pulsar beam is modified. As expected, it will be noticeable only near the stellar surface. For simplicity in this section we consider only “bending” without incorporating “squeezing.” For light bending we need to consider the null geodesics. We consider equations of motion for a photon propagating in both the Schwarzschild and Kerr background metrics. First let us discuss the Schwarzschild case. Because of the spherical symmetry of the Schwarzschild metric, there is no loss of generality if the geodesic is assumed to lie in the equatorial plane. In that case the polar terms in the metric can be dropped. This amounts to identifying θ_g with φ' and setting $\theta_g = \pi/2$. The angle φ_g then corresponds to the magnetic θ' . Photons emanating from a point r_e near the neutron star at an angle μ'_e with respect to the radius vector suffer gravitational bending away from the radial direction, which results in the beam divergence. The angle of emergence of the photon reaching a remote observer with respect to his radius vector is

$$\mu'_e(\infty) = \int_{r_e}^{\infty} \frac{d\varphi_g/d\Gamma}{dr/d\Gamma} dr, \quad (62)$$

where Γ is an affine parameter. In the Schwarzschild background, the geodesic equations can be solved (see, e.g., Chandrasekhar 1983) to give the photon 4-velocity components $d\varphi_g/d\Gamma$ and $dr/d\Gamma$, so that

$$\mu'_e(\infty) = \int_{r_e}^{\infty} \frac{q dr}{r^2 [1 - (1 - 2m/r)(q^2/r^2)]^{1/2}}, \quad (63)$$

where q is the so-called impact parameter of the photon. For a photon emitted from r_e at an angle μ'_e with respect to the radial direction,

$$q = q_0 \sin \mu'_e = \frac{r_e \sin \mu'_e}{(1 - 2m/r_e)^{1/2}}. \quad (64)$$

Thus it is seen that the effect of “bending” is to replace the tangent angle μ'_e by $\mu'_e(\infty)$, resulting in a divergence of the beam. The angles (θ'_r, φ'_r) describing the beam are now replaced by (θ'_b, φ'_b) , such that

$$\theta'_b = \theta'_e + \mu'_e(\infty), \quad (65)$$

$$\varphi'_b = \varphi'_c, \quad (66)$$

where we use the subscript b to denote bending. Like “squeezing,” “bending” also depends only on m/r_e and not on P , α , or B_0 . For $M = 1.4 M_\odot$ and $R_* = 10$ km, as is easy to estimate, the inclusion of light bending widens the pulsar beam by about 11% at the stellar surface. For a typical case this is illustrated in Figure 8. For $r_e = 2R_*$, the widening reduces to 4.3%. For emission altitudes larger than $5R_*$, it is $\leq 1.5\%$.

In order to determine the effect of spacetime curvature on the beamwidth in the presence of rotation, we have also considered the Kerr metric. This makes the bending calculation prohibitively complicated, as the light propagation is no

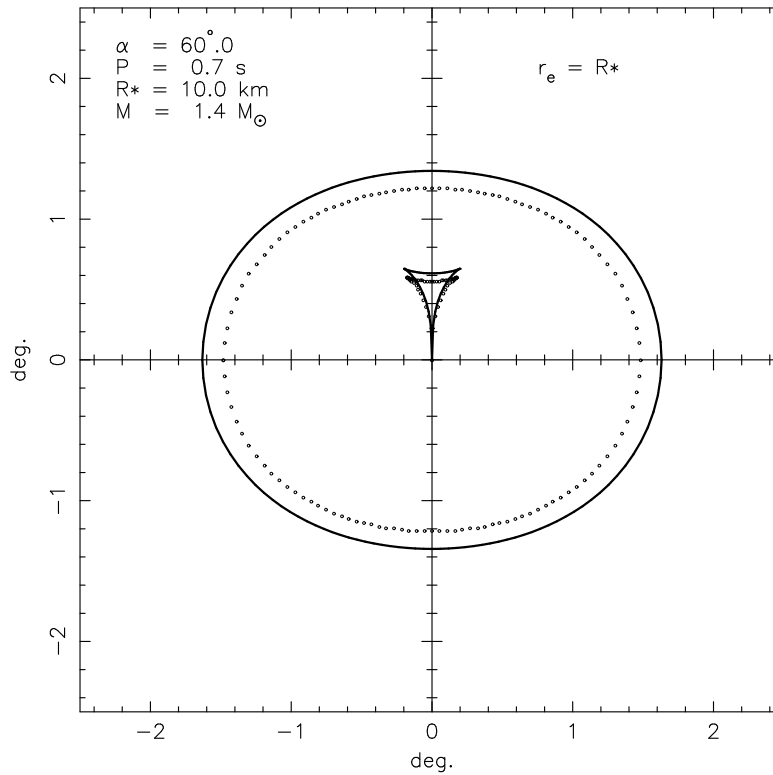


FIG. 8.—The inner curve (dots) is the flat spacetime polar cap. The outer curve (solid line) shows the polar cap widened due to the gravitational light bending. The stellar mass and radius are $1.4 M_\odot$ and 10 km, respectively.

longer planar. However, for values of the rotational parameter a , relevant for fast pulsars, it suffices to use the Kerr metric in its weak form. This means neglecting a^2 terms in the Kerr metric, compared to terms linear in a . For the sake of completeness we have evaluated bending using the weak Kerr metric under the assumption that geodesics are confined to the equatorial plane. The integrand in the bending integral equation (62) now is

$$\frac{d\phi_g}{dr} = - \frac{\omega(1 + \omega q) - q/r^2}{[(1 + \omega q)^2 - r^{-2}(1 - 2m/r)q^2]^{1/2}}, \quad (67)$$

where ω is the angular velocity of dragging of inertial frames given by

$$\omega = \frac{2J}{r^3} \quad (68)$$

and J is the specific angular momentum of the neutron star. The plots similar to Figure 8 using the Kerr metric are indistinguishable from their Schwarzschild counterparts even at $r_e = R_*$ and more so at higher altitudes. Henceforth we effect light bending using only the Schwarzschild metric.

8. COMBINATION OF “SQUEEZING” AND “BENDING”

Both “squeezing” and “bending” need to be included to consistently incorporate the general relativistic effects. This can be done easily by combining the procedures described in §§ 6 and 7. In equation (64) μ'_e is now replaced by μ'_E (see eq. [57]), leading to $\mu'_E(\infty)$ as the resultant in this case. As a consequence, equations (65) and (66) are changed to

$$\theta'_B = \theta'_E + \mu'_E(\infty), \quad (69)$$

$$\phi'_B = \phi'_E. \quad (70)$$

To summarize, in the absence of “squeezing” and “bending” the emission cone is described by equations (14)–(16). When field squeezing is included, these relations change over to equations (57)–(59), which are essentially equivalent to equations (14)–(16). If only “bending” is effected, then the corresponding quantities are described by equations (63)–(66). Inclusion of both the effects is described by equations (69) and (70). The opposing nature of “squeezing” and “bending” results in an overall squeeze of the flat spacetime beam by 4% at the surface of a star with $M = 1.4 M_\odot$ and $R_* = 10$ km. For $r_e = 2R_*$ and $5R_*$, the corresponding figures are 2.4% and 1.0%, respectively.

9. ABERRATION IN CURVED SPACETIME

Now we consider how all the kinematical effects can be combined. In order to include aberration in the curved spacetime case, we evaluate θ'_E , μ'_E , and θ'_R as in equations (57)–(59) so that field squeezing is taken care of. One can then find θ_R and ϕ_R

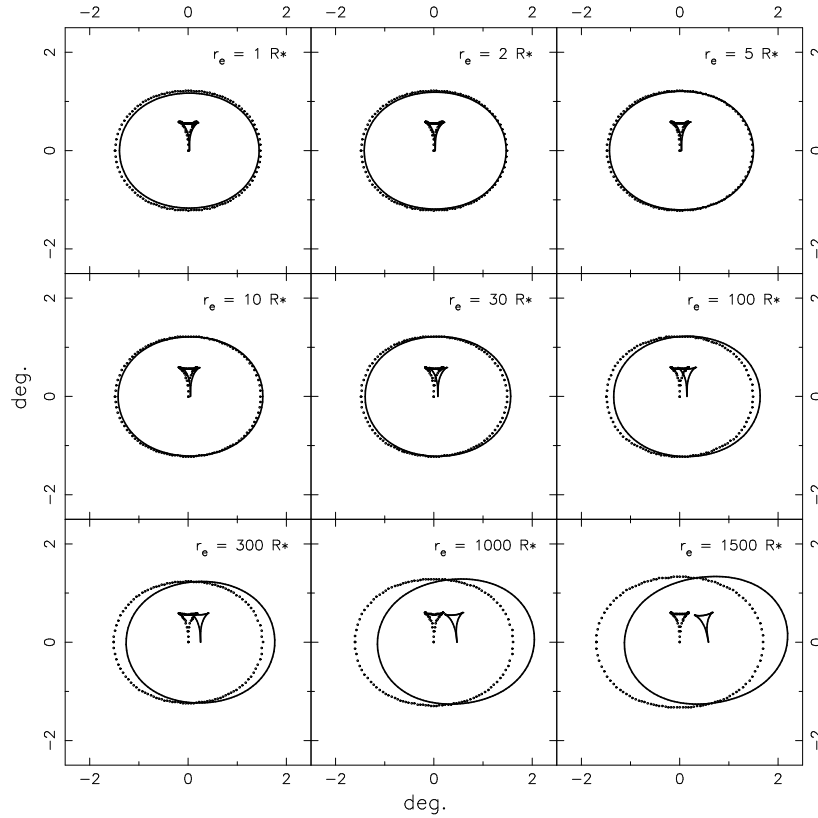


FIG. 9.—Emission cones for $\alpha = 60^\circ$, $P = 2^{-1/2}$ s, $R_* = 10.0$ km, $M = 1.4 M_\odot$, with “squeezing,” aberration, and “bending” (solid line) and without any of these (dots) for various altitudes as labeled. Angular extents are multiplied by $(R_*/r_e)^{1/2}$.

by transforming to rotational coordinates. Aberration is to be performed at this stage before bending is effected. Instead of equation (24), we use

$$v_g = \frac{r_e \Omega}{c} \left(1 - \frac{2m}{r_e}\right)^{-1/2} \sin \theta_E \quad (71)$$

as the corotation velocity. We then construct $\hat{\theta}_R$, $\hat{\phi}_R$, and finally $\hat{\theta}'_R$, $\hat{\phi}'_R$ as in § 4. It may be remembered that in the absence of aberration and light bending the radiation would propagate to a distant observer in the direction (θ'_R, ϕ'_R) . If aberration is taken into account, this direction changes to $(\hat{\theta}'_R, \hat{\phi}'_R)$. While propagating in the stellar gravitational field, however, the radiation finally reaches a distant observer in the direction $(\hat{\theta}'_B, \hat{\phi}'_B)$.

The effect of light bending described in § 8 (eqs. [69] and [70]) amounts to a simple operation of replacing μ'_E by $\mu'_E(\infty)$. This simplicity came about as a result of the exploitation of the spherical symmetry of the Schwarzschild spacetime, which allowed the option of considering the geodesics to lie in the equatorial plane. This simplification can still be utilized, but some modifications are necessary. If we still take the geodesics to lie in the equatorial plane of the Schwarzschild coordinates, i.e., $\theta_g = \pi/2$, then in terms of the magnetic coordinates it is the plane containing the radial direction (θ'_E, ϕ'_E) , the unbent aberrated photon velocity $(\hat{\theta}'_R, \hat{\phi}'_R)$, and the emergent photon velocity $(\hat{\theta}'_B, \hat{\phi}'_B)$. The transformation of Cartesian coordinates from the Schwarzschild to the magnetic ones is carried out by the rotation matrix R given below. This rotation matrix transforms the magnetic coordinates of a direction (θ', ϕ') to its Schwarzschild coordinates (θ_g, ϕ_g) such that $\theta_g = \pi/2$. The Schwarzschild azimuths ϕ_g of the above three directions are respectively ϕ_{gE} , $\hat{\phi}_{gR}$, and $\hat{\phi}_{gB}$. Without loss of generality we can take $\phi_{gE} = 0$. Now $\hat{\phi}_{gR}$ and $\hat{\phi}_{gB}$ are given by

$$\hat{\phi}_{gR} = \phi_{gE} + \mu'_A = \mu'_A, \quad (72)$$

$$\hat{\phi}_{gB} = \phi_{gE} + \mu'_A(\infty) = \mu'_A(\infty), \quad (73)$$

where μ'_A , the angle between the radial direction and the “squeezed,” aberrated, but unbent ray, is given by

$$\cos \mu'_A = \cos \theta'_E \cos \hat{\theta}'_R + \sin \theta'_E \sin \hat{\theta}'_R \cos(\phi'_E - \hat{\phi}'_R), \quad (74)$$

and the angle $\mu'_A(\infty)$, to which μ'_A changes after “bending,” is

$$\mu'_A(\infty) = \int_{r_e}^{\infty} \frac{\hat{q} dr}{r^2 [1 - (1 - 2m/r)(q^2/r^2)]^{1/2}}, \quad (75)$$

where with q_0 as in equation (64), the impact parameter to be used now is

$$\hat{q} = q_0 \sin \mu'_A. \quad (76)$$

A remote observer receives the radiation in the $(\theta_g = \pi/2, \varphi_g = \hat{\varphi}_{gB})$ direction. In magnetic coordinates this direction is described by $(\hat{\theta}'_B, \hat{\varphi}'_B)$, and the magnetic coordinates can be obtained by applying the inverse rotation matrix R^{-1} to Schwarzschild coordinates as follows:

$$\begin{pmatrix} \sin \hat{\theta}'_B \cos \hat{\varphi}'_B \\ \sin \hat{\theta}'_B \sin \hat{\varphi}'_B \\ \cos \hat{\theta}'_B \end{pmatrix} = R^{-1} \begin{pmatrix} \cos \mu'_A(\infty) \\ \sin \mu'_A(\infty) \\ 0 \end{pmatrix}. \quad (77)$$

The expressions for $\hat{\theta}'_B$ and $\hat{\varphi}'_B$ are no more simple. Note that $R^{-1} = R^T$ and R is equal to

$$\begin{pmatrix} \sin \theta'_E \cos \varphi'_E & \sin \theta'_E \sin \varphi'_E & \cos \theta'_E \\ -\cos \theta'_E \cos \varphi'_E \cos \Psi - \sin \varphi'_E \sin \Psi & -\cos \theta'_E \sin \varphi'_E \cos \Psi + \cos \varphi'_E \sin \Psi & \sin \theta'_E \cos \Psi \\ -\cos \theta'_E \cos \varphi'_E \sin \Psi + \sin \varphi'_E \cos \Psi & -\cos \theta'_E \sin \varphi'_E \sin \Psi - \cos \varphi'_E \cos \Psi & \sin \theta'_E \sin \Psi \end{pmatrix}, \quad (78)$$

where Ψ is given by

$$\sin \Psi = \frac{\sin \hat{\theta}'_R \sin (\hat{\varphi}'_R - \varphi'_E)}{\sin \mu'_A}. \quad (79)$$

The above method of effecting aberration in curved spacetime can be used also for the equatorial geodesics in the Kerr geometry. For emission altitudes beyond $5R_*$, the gravitational effects, namely, the field line squeezing and light bending, become negligible, while it is only for high emission altitudes that aberration becomes effective. Therefore, for slow pulsars, these effects can be treated separately as done in the previous sections. It is only for fast (millisecond) pulsars that the formalism of this section becomes relevant. We intend to discuss the kinematics of beams of fast pulsars elsewhere. The changes in the emission cone after inclusion of all effects (i.e., “squeezing,” aberration, and “bending”) are illustrated in Figure 9 for a typical long-period pulsar for various values of r_e . In these figures, light bending is done as for equatorial geodesics in the weak Kerr geometry, although they are indistinguishable from the corresponding Schwarzschild equivalents.

10. DISCUSSION

In this paper we have investigated the pulsar beam shapes obtainable in the polar cap model in a more complete manner than has been done so far. The effects related to the inclination angle α between the magnetic dipole and rotation axes, the effect of special relativistic aberration due to the corotation velocity of the sources, and the effect of stellar gravitation on the dipole magnetic field geometry and light propagation have been described in the previous sections. We now discuss them in the same order and assess their importance for pulsar phenomenology.

The dependence of the full emission cone shape on α has been discussed before, and as noted earlier (Biggs 1990), the latitudinal extent of the emission cone is seen to decrease as α varies from 0 to $\pi/2$. This dependence on α is, however, not very sensitive. The ratio of latitudinal to longitudinal extent, R_c , varies from 1 ($\alpha = 0$) to 0.62 ($\alpha = \pi/2$). What we find interesting is that the open field line region is necessarily determined by two branches of open field lines. The branches are distinguished only mathematically. However, the θ_c^+ part of the polar cap seems naturally relevant as the zone from which the core component of a pulsar pulse originates, while the conal component can be associated with the θ_c^- region (Kapoor & Shukre 1996, hereafter KS I). If such an identification is made, then because of the sensitive dependence of the θ_c^+ region on α , one would expect a strong α dependence to be manifested in core emission. We have discussed this elsewhere (KS III).

Recently Blaskiewicz et al. (1991) dealt with the effect of aberration on the pulsar radio emission. They treated it as a dynamical feature of the radiation, and to order v^2 . In contrast, we treat it as a kinematical effect, and exactly. As seen in our Figure 6, and found by Blaskiewicz et al. (1991), the analysis of linear polarization position-angle swings through radio pulses will be affected by aberration. Until an analysis similar to that of Blaskiewicz et al. (1991) is performed using our formalism, no further conclusions can be drawn.

We wish, however, to make the following comments concerning the role of aberration in pulsar pulse widths. In the so-called “light cylinder” model of pulsar emission (see Manchester & Taylor 1977) the narrowness of the pulsar beam is a consequence of an extreme amount of aberration occurring due to corotation velocities very close to the speed of light. In the context of the polar cap model, radiation is usually considered to originate from near the star. However, if we take the polar cap model literally, and follow a bunch of open field lines away from the star, the extent of the emission zone will increase roughly as $r_e^{1/2}$. Because of the consequent increase in corotational velocity, one would naively have expected reduction in the apparent size of the emission cone. This does not happen if the full extent of the emission cone is considered as noted at the end of § 3. The upper limit of $r_e = \frac{2}{3}r_{LC}$ for the emission altitude is maintained in this case even after aberration is included. This restriction can be circumvented if only a very small portion of the emission cone, such as the θ_c^+ region, is active. If different components of the pulsar pulse originate at different altitudes, the relative aberration can introduce a phase shift between them within the pulse. In KS I we have attributed the core emission to the θ_c^+ region, which necessitates higher emission altitudes for the core components compared to the conal ones. This will imply a phase difference between the centers of the core and conal components, as is observationally often seen (Lyne & Manchester 1988; Rankin, Stinebring, & Weisberg 1989). The net shift is a result of the opposing contributions from aberration and magnetic field line sweepback (MFS) (Shitov 1985). An investigation of these effects leads to new interrelations among pulsar parameters, such as the emission altitude and the inclination angle α (KS III).

The effect of the stellar gravitational field on the dipole magnetic field is to “squeeze” it. This has been described in § 6 for a general inclination angle α . At $r_e = R_*$, this leads to a 14% shrinking of the emission cone. However, at $r_e = 2R_*$ it reduces to 6.5% and to only 2.5% at $r_e = 5R_*$. Thus it is not significant for altitudes beyond $5R_*$. It should be borne in mind that this

effect as well as the light bending mentioned below depend only on the ratio M/r_e and not on the period P , the surface magnetic field strength B_0 , or the inclination angle α . The effect of light bending is opposite to that of field “squeezing” and widens the beam. The effect of the stellar rotation as incorporated through the use of the weak Kerr metric is totally insignificant. We have thus effected light bending using the Schwarzschild metric and for all values of α . At the stellar surface $r_e = R_*$, the beam is widened by 11%. However, at $r_e = 2R_*$ this figure is reduced to 4.3%, and to 1.5% at $r_e = 5R_*$. Thus it also is insignificant for altitudes beyond $5R_*$. The net effect after combining “squeezing” and “bending” results in a slight squeeze of the emission cone which for any α and r_e is at most 4% of its flat spacetime value. It is $\leq 2.4\%$ beyond $r_e \cong 2R_*$. Because of the small size of the net effect, the expressions for the compression and elongation ratios R_c and R_c^+ (see eqs. [17] and [20]) still remain valid. Also, this no longer allows us to conclude rigorously that the core emission cannot emanate from the stellar surface as was claimed in KS I.

We now present in a nutshell the assessment of the impact of the various effects considered here on changing the pulsar beam shapes. The general relativistic effects due to “squeezing” and “bending” in combination are very small even at the stellar surface, owing to their opposing nature. This will be true for all pulsars irrespective of their period and magnetic field. The effect due to aberration could be noticeable at high emission altitude but will be countered by the opposing effect due to MFS. Thus, surprisingly, the Goldreich-Julian type beam is essentially unaltered by these effects. That the emission altitudes below $\frac{2}{3}r_{LC}$ alone are meaningful if the full emission cone is considered still remains true. It would be of interest to study the interplay between aberration and MFS in some models. At a finer level these effects may be noticeable in observations, and we will report on these investigations for long-period pulsars in KS III. However, the picture may be more complex for short-period pulsars. Notice that for the 1.5 ms pulsar $r_{LC} = 7.5R_*$. Therefore, even for $r_e \lesssim \frac{2}{3}r_{LC}$, individually none of the above effects need be negligible. The mutual cancellations will, however, make the net effect small, although the interplay between them and its consequent signature in pulses will vary from one to the other short-period pulsar. We expect this to show up in profiles of millisecond pulsars and to shed light on the elusive details of the pulsar emission. We shall deal with this elsewhere.

C. S. S. would like to thank B. R. Iyer and J. Samuel for discussions on geodesics. R. C. K. thanks Baba Varghese and J. Nathan for software help.

REFERENCES

- Arons, J. 1979, *Space Sci. Rev.*, 24, 437
 ———. 1993, *ApJ*, 408, 160
 ———. 1996, in *IAU Colloq. 160, Pulsars: Problems and Progress*, ed. S. Johnston, M. A. Walker, & M. A. Bailes (San Francisco: ASP), 177
 Biggs, J. D. 1990, *MNRAS*, 245, 514
 Blaskiewicz, M., Cordes, J. M., & Wasserman, I. 1991, *ApJ*, 370, 643
 Chandrasekhar, S. 1983, *The Mathematical Theory of Black Holes* (Oxford: Oxford Univ. Press)
 Chen, K., & Ruderman, M. A. 1993, *ApJ*, 408, 179
 Chitre, D. M., & Vishweshvara, C. V. 1975, *Phys. Rev. D*, 12, 1538
 Ginzburg, V. I. 1964, *Dokl. Akad. Nauk SSSR, Ser. Astron.*, 156, 43
 Goldreich, P., & Julian, W. H. 1969, *ApJ*, 157, 869
 Gonthier, P. L., & Harding, A. K. 1994, *ApJ*, 425, 767
 Kapoor, R. C. 1991a, *ApJ*, 378, 227
 ———. 1991b, poster paper presented at Int. Conf. on Gravitation and Cosmology (Ahmedabad, 1991 December)
 Kapoor, R. C., & Shukre, C. S. 1995, *Bull. Astron. Soc. India*, 23, 477
 ———. 1996, in *IAU Colloq. 160, Pulsars: Problems and Progress*, ed. S. Johnston, M. A. Walker, & M. Bailes (San Francisco: ASP), 229 (KS I)
 ———. 1998, in preparation (KS III)
 Kijak, J., & Gil, J. 1997, *MNRAS*, 288, 631
 Lyne, A. G., & Manchester, R. N. 1988, *MNRAS*, 234, 477
 Manchester, R. N., & Taylor, J. H. 1977, *Pulsars* (San Francisco: Freeman)
 Melrose, D. B. 1992, in *IAU Colloq. 128, The Magnetospheric Structure and Emission Mechanisms of Radio Pulsars*, ed. T. H. Hankins, J. M. Rankin, & J. A. Gil (Zielona Gora, Poland: Pedagogical Univ. Press), 304
 Michel, F. C. 1992, in *IAU Colloq. 128, The Magnetospheric Structure and Emission Mechanisms of Radio Pulsars*, ed. T. H. Hankins, J. M. Rankin, & J. A. Gil (Zielona Gora, Poland: Pedagogical Univ. Press), 405
 Petterson, J. A. 1974, *Phys. Rev. D*, 10, 3166
 ———. 1975, *Phys. Rev. D*, 12, 2218
 Phillips, J. A. 1992, *ApJ*, 385, 282
 Radhakrishnan, V., & Cooke, D. J. 1969, *Ap. Letters*, 3, 225
 Rankin, J. 1990, *ApJ*, 352, 247
 ———. 1993, *ApJ*, 405, 285
 Rankin, J., Stinebring, D. R., & Weisberg, J. M. 1989, *ApJ*, 346, 869
 Roberts, D. H., & Sturrock, P. A. 1972, *ApJ*, 172, 435
 Scharlemann, E. T., Arons, J., & Fawley, W. M. 1978, *ApJ*, 222, 297
 Shitov, Yu. P. 1985, *Soviet Astron.*, 29, 33
 Sturrock, P. A. 1971, *ApJ*, 164, 529
 Wasserman, I., & Shapiro, S. L. 1983, *ApJ*, 265, 1036